Solar Energy Materials & Solar Cells 95 (2011) 2141–2150

Contents lists available at ScienceDirect

Solar Energy Materials & Solar Cells

journal homepage: www.elsevier.com/locate/solmat

Exploiting optical anisotropy to increase the external quantum efficiency of flexible P3HT:PCBM blend solar cells at large incident angles

Shang-Yu Chuang, Chen-Chieh Yu, Hsuen-Li Chen *, Wei-Fang Su, Chun-Wei Chen

Department of Materials Science and Engineering, National Taiwan University, No. 1, Section 4, Roosevelt Road, Taipei 10617, Taiwan

ARTICLE INFO

Article history:
Received 12 January 2011
Accepted 8 March 2011
Available online 31 March 2011

Keywords:
P3HT/PCBM blend
Optical anisotropy
Various incident angle operation
Flexible solar cells
Moth-eye structures
External quantum efficiency

ABSTRACT

The external quantum efficiencies of P3HT:PCBM blend solar cells decrease significantly when they are bent or illuminated at large incident angles because of (i) optical anisotropy of the P3HT:PCBM films—primarily because a mismatch between the direction of the electric field of the incoming light and the orientation of the P3HT:PCBM blend nanocrystallites results in a significant reduction in the amount of TM-polarized light absorbed and (ii) interfacial reflection of multilayer structures – primarily because the outermost air–flexible substrate interface exhibits a distinct refractive index difference – at large incident angles. Textured moth-eye structures fabricated by nanoimprint lithography on the flexible substrates of organic solar cells reduce the degree of interfacial reflection at high incident angles; they should allow more TE-polarized light to absorb in the P3HT:PCBM films (active layers) of the organic solar cells.

1. Introduction

Much attention is focused at present on research into photovoltaic devices, with the goal of exploiting solar light as a next-generation energy source [1–3]. The most popular photovoltaic devices are Si-based solar cells—because techniques for their manufacture are mature and they can exhibit high efficiency. The inflexibility and opacity of Si-based solar cells are, however, limitations on their applicability. Because flexible photovoltaic devices are less likely to fracture when bent, they have greater potential in a wide range of applications. Organic photovoltaics (OPVs) are promising candidates for use in flexible photovoltaic devices because they are polymer-based and can be fabricated on flexible substrates [4–8]. Moreover, OPVs can be prepared at low-cost, with high throughput, at low processing temperatures. The poly(3-hexylthiophene): 6,6-phenyl-C61-butyric acid methyl ester (P3HT:PCBM) blend is the most commonly used material applied to OPVs because of its chemical stability and high crystallinity, carrier mobility, and absorption. Nevertheless, OPVs have much lower efficiencies relative to their inorganic counterparts. The maximum power conversion efficiency (PCE) of an OPV based on P3HT:PCBM is ca. 5%—considerably less than those of Si-based devices [9,10]. The limited device efficiency of OPVs has not, however, affected their development because their most outstanding feature – flexibility – makes them particularly attractive to the solar energy industry [11–13].

To enhance the efficiency of OPV-based solar cells, much attention has been focused on improving their material [14,15], electrical properties [16,17] and architectures [18,19]. Most of these approaches, however, fail to take into account the effect of bending a flexible OPV or operating it at wide incident angles. The internal and external quantum efficiencies are two important factors affecting device performance. The internal quantum efficiency of a solar cell depends on its intrinsic material properties [20], such as its crystallinity, energy band gap, carrier transport behavior, and the number of defects and impurities. The external quantum efficiency is associated with the solar cell's interfacial reflection, photon absorption, and architecture, which all affect the number of collected electron/hole pairs. Therefore, the efficiency of a flexible OPV will be affected by its bending and/or illumination at different incident angles.

A bent organic solar cell encounters light from various incident angles—as does a flat solar cell during the day, due to the motion of sun. For the latter, a sun-tracking system is one solution to the projected area (cosine) effect and to reduce the degree of interfacial reflection at oblique incident angles [21]. The energy consumed by a sun-tracking system would, however, be impractical when using low-efficiency organic solar cells. Therefore, organic solar cells will inevitably experience sunlight from a wide range of angles; no apparent solutions to this problem have been reported previously. The incident angle affects the external quantum efficiency for two main reasons:

(i) *Reflection at multiple interfaces*: The reflectance at an interface depends on the refractive index difference between the two media and also on the incident angles. A large refractive index difference or a large oblique incident angle will result in an

* Corresponding author. Tel.: +886 2 33663240; fax: +886 2 23634562.
E-mail address: hsuenlichen@ntu.edu.tw (H.-L. Chen).

0927-0248/$ - see front matter © 2011 Elsevier B.V. All rights reserved.
doi:10.1016/j.solmat.2011.03.015

intense reflection, thereby reducing the amount of light transmitted into the active layer and, consequently, decreasing the external quantum efficiency. For a bent solar cell, the incoming light arrives from a wide range of incident angles. In addition, polarized light exhibits different interfacial reflection behavior – and, therefore, different transmittance – depending on its incident angle.

(ii) *Optical anisotropy of P3HT:PCBM blend films*: The anisotropic properties of P3HT:PCBM blends, based on the preferred orientation of the polymer nanocrystallites, strongly influence the carrier mobility and optical absorption [22–30]. We define the direction of electric field oscillation of light parallel (TE-polarized) and perpendicular (TM-polarized) to the substrate. Incident light having its electric field aligned parallel to the polymer main chains – i.e., the orientation of the transition dipole moments – will result in $\pi-\pi^*$ absorption [31]. Thus the optical properties become anisotropic when there is a high degree of main chain alignment and extension. There are three possible crystalline orientations of P3HT:PCBM thin films [32], with the most preferred having the main chains of polymer nanocrystallites aligned parallel to the surface. If the electric field of the incident light is parallel to this preferred main chain orientation, the absorption of light will be significant. Therefore, TE- and TM-polarized rays of light exhibit different absorption behavior because of the perpendicular and parallel directions, respectively, of their electric fields with respect to the alignment of the polymer main chains. Measuring the reflectance and transmittance spectra of polarized light over a range of incident angles reveals the optical anisotropic properties of P3HT:PCBM blends [28].

In this study, we examined the influence of bending (radius of curvature) and irradiation at oblique incident angles on the external quantum efficiencies of flexible OPVs. To characterize the external quantum efficiency loss, we measured the transmittances and reflectances at the multiple interfaces using different types of polarized light over a wide range of incident angles. The influences of the regioregularity (RR) and annealing temperature on optical anisotropy have been reported previously in our researches [28]. Here, we demonstrate that optical anisotropy leads to obvious anisotropy of absorption for organic solar cells. This phenomenon reduces the efficiency of OPVs toward TM-polarized light at large incident angles. Furthermore, the reflectance of TE-polarized light increases dramatically upon increasing the incident angle. Both factors reduce the external quantum efficiency of OPV when illuminated at large incident angles. Finally, we suggested textured flexible substrates fabricated by nanoimprint lithography to effectively enhance the efficiency of OPVs at oblique angles.

2. Experimental section

P3HT polymers were synthesized using the Merck synthetic method. The blend film was prepared from a solution of P3HT and PCBM (1:0.8, w/w) in chlorobenzene (CB). The P3HT:PCBM films were spun at 800 rpm for 60 s and then thermally annealed. All optical spectra were measured using a Hitachi U-4000 optical spectrometer. The optical constants – namely, the refractive index (n) and the extinction coefficient (k) – of the P3HT:PCBM films were determined using an ellipsometer and from transmittance

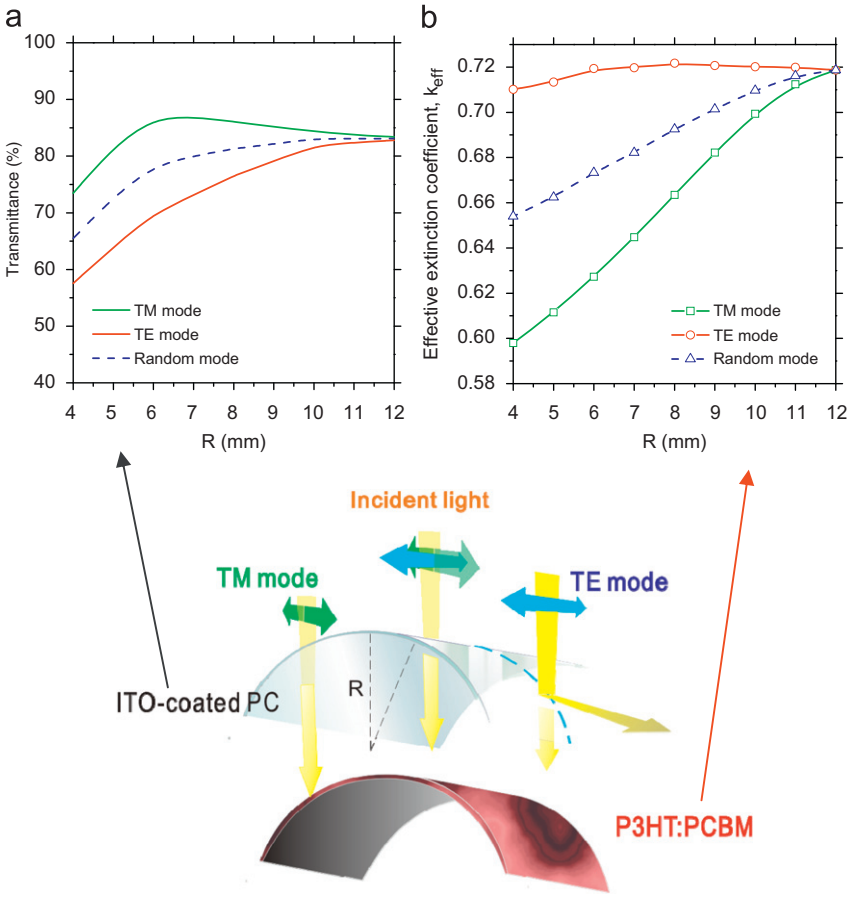

Fig. 1. (a) Transmittance of an ITO-coated substrate bent at various radii of curvature. (b) Effective extinction coefficients of a P3HT:PCBM blend film coated on a PC substrate bent at various radii of curvature (for interpretation of the references to color in this figure legend, the reader is referred to the web version of this article).

and reflectance spectra. Optical spectra of the P3HT:PCBM films were measured using a Hitachi U-4100 optical spectrometer. X-ray diffraction (XRD) spectra of the P3HT:PCBM hybrid films before and after thermal annealing were measured using a GIXRD with synchrotron X-rays (out-of-plane scanning mode). To measure the photovoltaic device performance, solar cells were fabricated under ambient conditions. ITO substrates were etched with acid and then cleaned with $CHCl_3$, acetone, and deionized water in an ultrasonication bath. The cleaned ITO samples were immediately spin-coated at 1500 rpm with a 30-nm-thick layer of PEDOT:PSS. The PEDOT:PSS-coated samples were then heated at 110 °C for 5 min. The active layer of P3HT:PCBM (1:0.8) was spin-coated to form a thin film having a thickness of 80 nm. The samples were placed in a vacuum chamber, where an aluminum electrode (100 nm) was deposited through a mask; these samples were then annealed at 120 °C for 15 min. The photovoltaic device efficiency was measured under simulated AM1.5 illumination conditions. For fabrication of the antireflection structure, the Si mold was fabricated through electron beam lithography (Leica, Weprint-200) and subsequent reactive ion etching using a high-density-plasma reactive ion etching (HDP-RIE) system (Duratek, Mutiplex Cluster) equipped with an inductively coupled plasma (ICP) source. Direct nanoimprinting on the flexible PC substrate was performed for 3 min at a temperature of 150 °C and a pressure of 8 MPa.

3. Results and discussion

Fig. 1 displays the effect of curvature on the interfacial transmittance of indium tin oxide (ITO)-coated polycarbonate (PC) substrates and the effective extinction coefficient of a P3HT:PCBM blend film. We used a homemade apparatus to uniformly bend the flexible OPV and to allow the incident light to be distributed over the total area of the OPV. To characterize the influence of bending on the transparency of P3HT:PCBM-based organic solar cells, we used both non-polarized and polarized light (wavelength: 510 nm) to measure the transmittance and absorbance. Fig. 1a displays the transmittance of ITO-coated PC substrates (12 mm × 12 mm) bent at various radii of curvature. We observed 80% transmittance from the flat ITO/PC substrate (radius of curvature: ∞) under random polarized light. Its transmittance gradually decreased to 65% when the radius of curvature decreased to 4 mm. Next, we tested the transmittance of polarized light to characterize the optical behavior of the OPVs. The transmittance of TE-polarized light exhibited a similar decline as that of the randomly polarized light, decreasing from 80% to 57%. In contrast, the transmittance of TM-polarized light initially increased from 80% to 85% as the radius of curvature decreased from 12 to 6.5 mm and then decreased to 73% at 4 mm. This behavior suggests that (i) the decreased transmittance of TE-polarized light contributes greatly to the declining transmittance

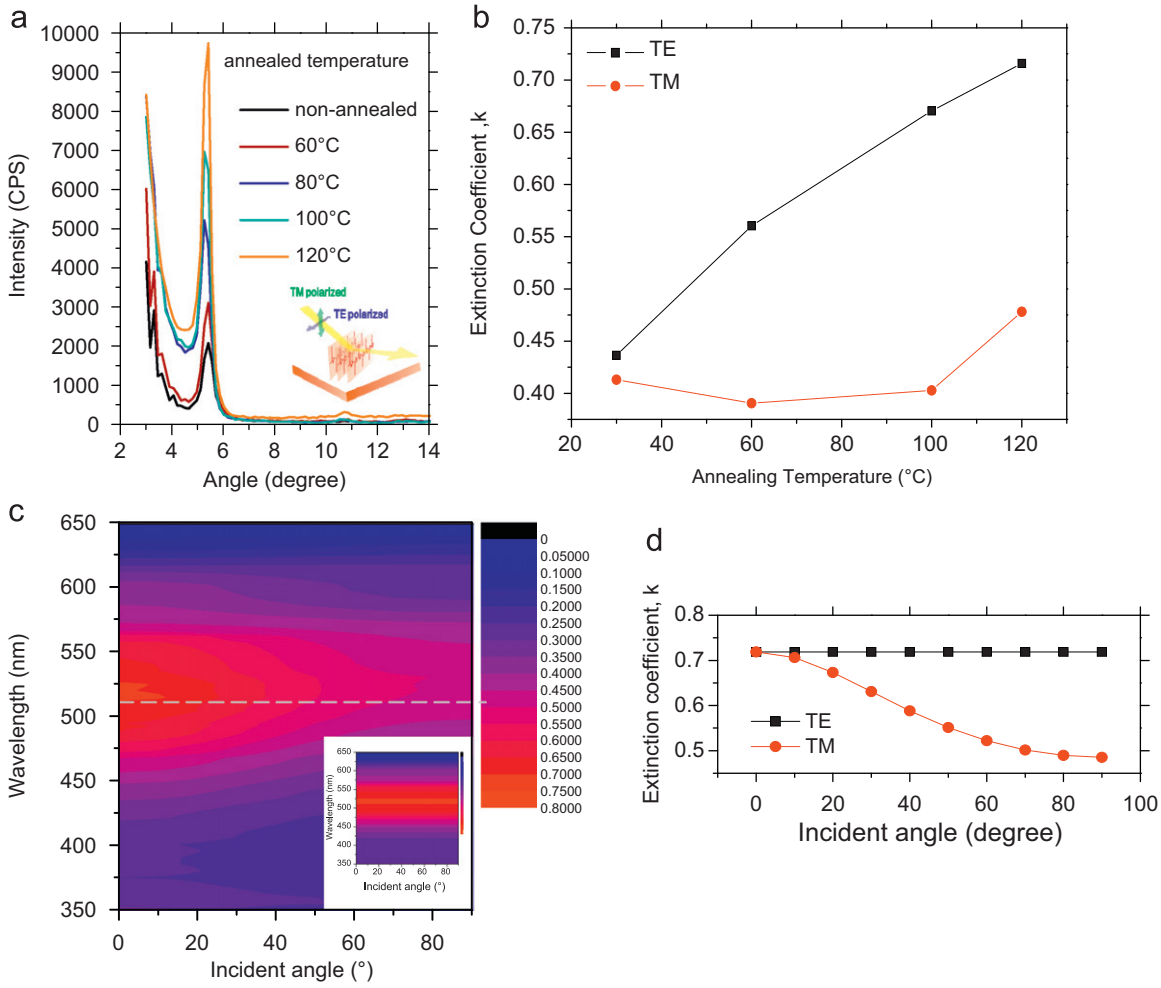

Fig. 2. (a) Grazing-angle X-ray diffraction spectra of P3HT:PCBM blend films prepared at various thermal annealing temperatures. (b) Extinction coefficients of 96.7%-RR P3HT:PCBM film under TE- and TM-polarized light after thermal annealing at various temperatures. (c) Extinction coefficient mapping under TM- and TE-polarized light for the film after thermal annealing at 120 °C. (d) Angle-dependent extinction coefficients of the film under TM- and TE-polarized light.

of random polarized light and (ii) severe bending causes ITO/PC substrates to exhibit relatively low transmittance as a result of their large reflectance.

Fig. 1b displays the effective extinction coefficients of a P3HT:PCBM blend (1:0.8, w/w) film coated on a flexible substrate bent at various radii of curvature. We determined the extinction coefficients of P3HT:PCBM blend films at 510 nm from reflectance–transmittance (R–T) and ellipsometry measurements and subsequent fitting of the measured reflectance and transmittance data to a dispersion function (an oscillator model describing the dielectric function). The extinction coefficient measured using randomly polarized light (blue line) decreased from 0.72 to 0.65 when the radius of curvature decreased from ∞ to 4 mm. Next, we determined the extinction coefficients of the film toward TM- and TE-polarized light over a range of radii of curvature. The effective extinction coefficient of the film under TM-polarized light (green line) decreased from 0.72 to 0.60 upon decreasing of radius of curvature. In contrast, for TE-polarized light, the film maintained an extinction coefficient of ca. 0.72 at all radii of curvature (red line). These measurements reveal that bending influences the degrees of interfacial transmittance and optical absorption of the active layer. The efficiency of a bent solar cell would suffer from light impinging on different positions of its curved substrate at various incident angles. Indeed, its absorption will be averaged from the contributions of each incident angle of light.

We measured the crystallinity of P3HT:PCBM blend films subjected to various thermal annealing treatments to investigate the effect of bending on their extinction coefficients. Many crystallization treatment processes such as thermal annealing and solvent annealing were applied for regaining the extended and aligned P3HT [28]. Because PCBM diffuses into larger aggregates during thermal processing, the P3HT chains can convert into crystallites in the PCBM-free regions [31]. To determine the effect of the annealing temperature on the polymer crystallinity, we used grazing-incidence X-ray diffraction (GIXRD; incident angle θ_{in}: 0.5°; wavelength: 1.027 nm) to measure the orientations of the polymer main chains in the P3HT:PCBM blend films (Fig. 2a). Thermal annealing induced the P3HT chains to crystallize and align in a more orderly manner. The main diffraction angle appeared at a value of 2θ of 5.4° for all of the P3HT:PCBM blend films; this diffraction angle corresponds to the diffraction of the crystallographic (1 0 0) plane of P3HT, suggesting that the preferred orientation of the crystalline P3HT was parallel to the substrate. The GIXRD spectra revealed that the diffraction intensity at a value of 2θ of 5.4° increased significantly upon increasing the annealing temperature; i.e., a greater number of P3HT chains adopted a crystalline orientation parallel to the substrate when annealed at higher temperatures.

Moreover, the anisotropic crystallinity of a P3HT:PCBM blend largely affects its optical absorption [28]. Thus, we used wide-angle

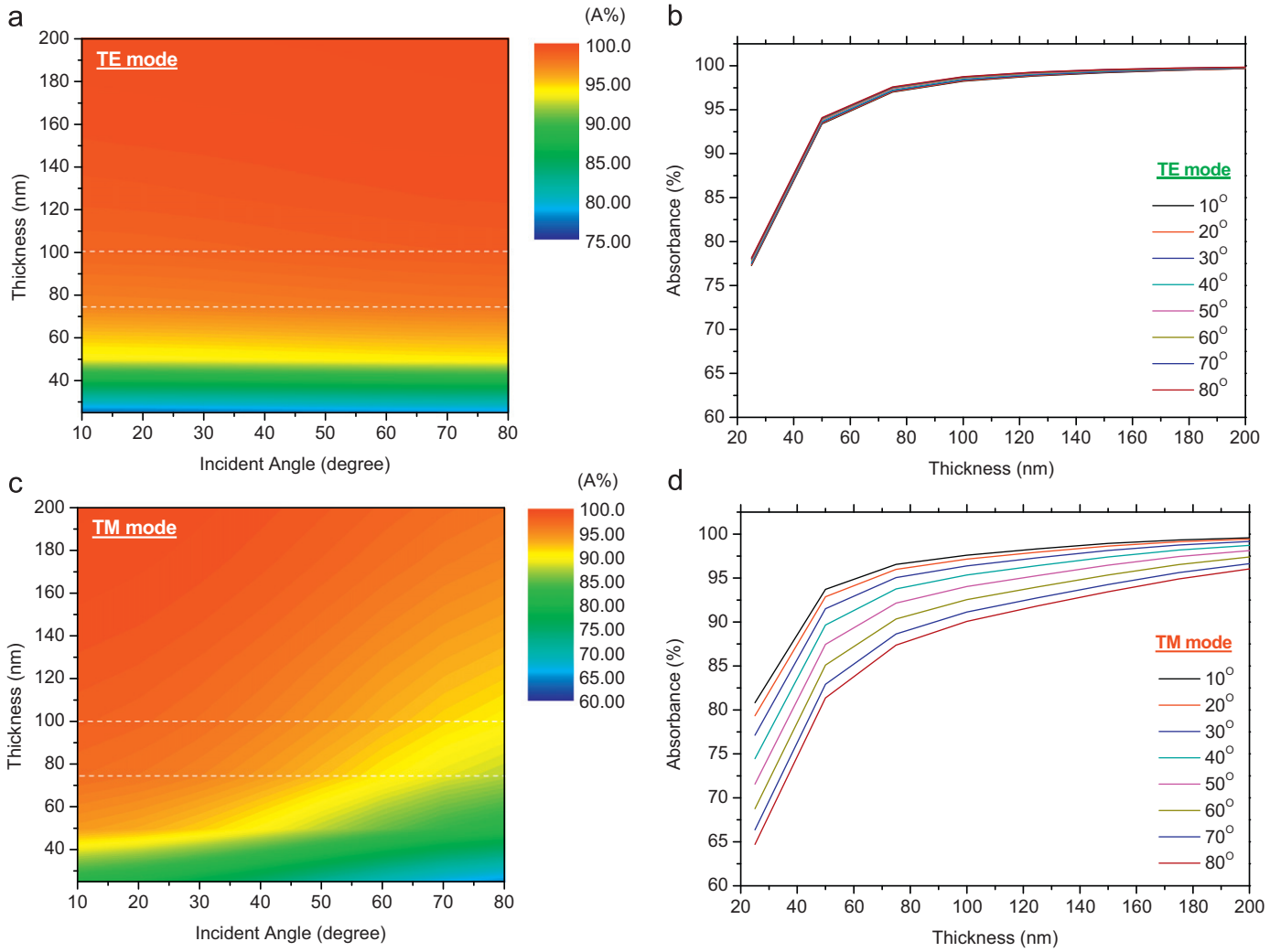

Fig. 3. The normalized absorbance mapping and normalized absorbance at 510 nm for active layer with different thicknesses and incident angles under (a) TE- and (b) TM-polarized light.

reflectance–transmittance measurements over a broad range of wavelengths (350–650 nm) to determine the extinction coefficients of the P3HT:PCBM films; the results were fitted to a dispersion function. The fitting method was based on a multilayer thin-film model [31,33]. Note that the calculated extinction coefficients correlated to intrinsic optical property of the P3HT:PCBM films and were not disturbed by the electric field profiles resulted from the interference effect. Fig. 2b presents the extinction coefficients of 96.7%-RR P3HT:PCBM films under TE-polarized (k_{TE}) and TM-polarized (k_{TM}) light at different annealing temperatures. As the annealing temperature increased from room temperature to 120 °C, the extinction coefficient under TE-polarized light increased from 0.44 to 0.73 whereas the one under TM-polarized light increased slightly from 0.42 to 0.47. The results obviously indicated that the annealing temperatures strongly influenced the anisotropic crystallinity of the P3HT:PCBM blend. Fig. 2c maps the extinction coefficients of P3HT:PCBM films under TE-polarized and TM-polarized light after annealing at 120 °C. The mapping reveals that the P3HT:PCBM blend exhibited maximum absorption peaks at 510 nm at normal incidence for both TE- and TM-polarized light. Larger incident angles led to smaller values of k_{TM}, whereas k_{TE} remained close to its maximum value over a broad range of incident angles. To investigate this behavior in detail, Fig. 2d presents the peak values of the extinction coefficients under TE- and TM-polarized light (510 nm) at incident angles ranging from 0° to 80°. Because bent solar cells are illuminated with incident light from a diverse range of angles, the incoming light would interact with various crystalline orientations of the P3HT:PCBM film. TE-polarized light would confront the same crystalline orientation of the P3HT:PCBM blend films, regardless of its incident angle, because its electric field is always aligned parallel to the substrate. Therefore, the extinction coefficient under TE-polarized light was maintained at ca. 0.72 for all incident angles. In contrast, TM-polarized light would confront different crystalline orientations of the P3HT:PCBM blend films at different incident angles because the direction of its electric field varies with respect to the incident angle. As indicated in Fig. 2d, the extinction coefficient under TM-polarized light was 0.72 at 0°, decreasing to 0.48 upon increasing the incident angle to 80°—i.e., as the electric field of the TM-polarized light became increasingly perpendicular to the substrate and fewer chains in the P3HT:PCBM blend were crystallized in this direction. Therefore, the varying of the extinction coefficient under bending, as indicated in Fig. 1b, was correlated to the anisotropic crystallinity of the P3HT:PCBM blend.

Next, we consider the absorbance of the P3HT:PCBM blend in an OPV. A multilayer thin-film model was used to calculate the absorbance of the P3HT:PCBM blend when an aluminum electrode was presented. The existence of the aluminum electrode led to a strong optical interference effect [34]. Optical interference would influence the amount of light that reached into the active layer, and thus resulted in different absorbance. Therefore, we calculated the absorbance of P3HT:PCBM blend fluctuates with different thicknesses. To further verify the absorption property of the P3HT:PCBM blend, we normalized our calculated absorbance to the penetrating light intensity. The normalized absorbance would correspond to the intrinsic absorption property of the P3HT:PCBM blend. Figs. 3a and b display the normalized absorbance mapping and peak values of the extinction coefficients (510 nm) for active layers of various thicknesses under oblique incidence of TE- and TM-polarized light, respectively. For the P3HT:PCBM blends having different thicknesses, the normalized absorbance under TE-polarized light illumination did not vary with various incident angles. The results were well agreeable with those in Fig. 2c. The phenomenon attributed to that the TE-polarized light had an electric field direction permanently parallel to the crystalline direction of P3HT, and thus k_{TE} would maintain a constant value at all incident angles. However, as displayed in Fig. 3b, the normalized absorbance under TM-polarized light decreased much at large angles in all thicknesses due to the optical anisotropy effect. The absorbance of the active layer under TE-polarized light did not decrease with various incident angles whereas the one under TM-polarized light declined largely at large incident angles. The simulation results gave us an inspiration that the optical anisotropy effect was still a significant issue in all P3HT:PCBM-based OPV even if the optical interference had been considered.

Moreover, we investigated the influence of the incident angle on the interfacial transmission and reflection. In our organic solar cells, incoming light would encounter four interfaces prior to reaching the active layer: the air–PC substrate, PC substrate–ITO, ITO–poly

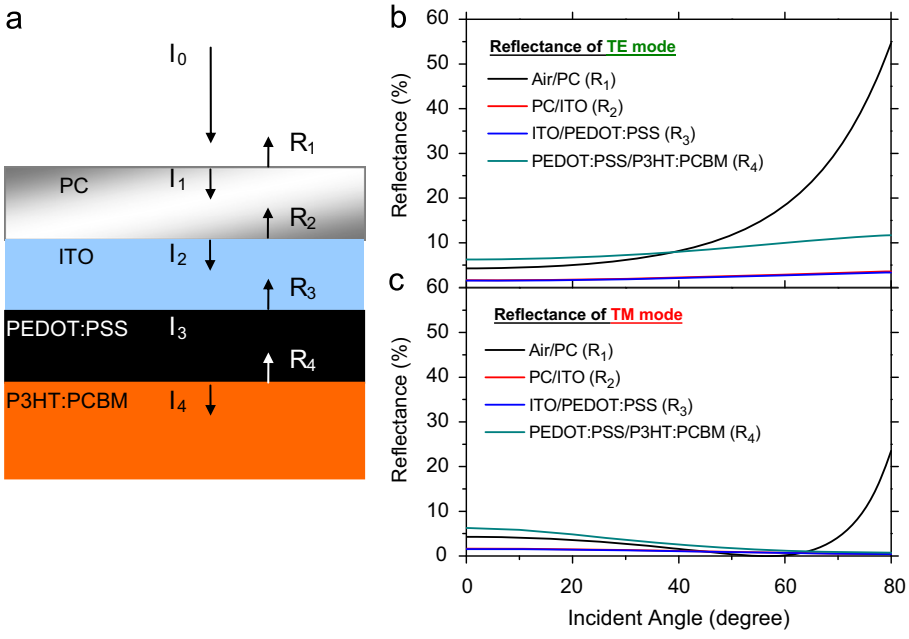

Fig. 4. (a) Multilayer structure of the P3HT:PCBM-based OPV. (b, c) Angle-dependent reflectance under (b) TE and (c) TM-polarized light.

(3,4-ethylenedioxythiophene):poly(styrenesulfonate) (PEDOT:PSS), and PEDOT:PSS–P3HT:PCBM interfaces. Fig. 4 displays the angle-dependent reflectances of the TE- and TM-polarized light at the various interfaces. When TE-polarized light (510 nm) encountered the outer air–PC substrate interface, its reflectance increased from 4% to 55% upon increasing the incident angle from 0° to 80°. The reflectance at each of the other interfaces, however, did not increase significantly, remaining less than 10% for all incident angles. The Fresnel equation of TE-polarized light is

$$R_{TE} = \left(\frac{n_i \cos\theta_i - n_t \cos\theta_t}{n_i \cos\theta_i + n_t \cos\theta_t}\right)^2 \quad (1)$$

where R is the reflectance of the TE-polarized light and n_i and n_t are the refractive indices of the media through which the incident and transmitted light travel, respectively. In our organic solar cell, the first reflection interface was positioned between air ($n=1$) and the PC substrate ($n=1.58$). This large difference in refractive index led to the large reflectance. Because the differences in refractive index at all of the other internal interfaces were relatively minor, no significant reflection occurred.

Fig. 4b displays the angle-dependent reflectance of TM-polarized light. The reflectance at the first interface (air–PC substrate) initially decreased upon increasing the incident angle, due to the Brewster angle effect. The Brewster angle is calculated according to the equation

$$\theta_B = \tan^{-1}\left(\frac{n_2}{n_1}\right) \quad (2)$$

For an air ($n=1$)–PC substrate ($n=1.58$) interface, the Brewster angle should be 57.7°, consistent with our measured result. Thus, the reflectance decreased initially to 0% at 57.7° and then rose to 23% at an angle of 80°. Similarly, because the differences in refractive index at the other internal interfaces were all small, their reflectances remained less than 3%, even at large incident angles. Our simulation suggests that part of the loss in efficiency of OPVs can be attributed to the reflection of TE-polarized light at the air–PC substrate interface at large incident angles.

To verify the effect of the incident angle on device efficiency, we measured the open circuit voltages (V_{OC}), short circuit current densities (J_{SC}), fill factors (FFs), and power conversion efficiencies (η) of P3HT:PCBM solar cells over a range of incident angles (Fig. 5). Solar cells having an area of 4 cm^2 and possessing layered structures in the configuration ITO (140 nm)/PEDOT (30 nm)/P3HT:PCBM (85 nm)/Al (100 nm) were fabricated in ambient air. We measured the current density–voltage (J–V) characteristics of the P3HT:PCBM blend devices under illumination with a simulated AM1.5 light source. Figs. 5a and b display the measured values of V_{OC} and FF under TE- and TM-polarized light, respectively. The values of V_{OC} under the TE- and TM-polarized light were both ca. 0.54 V, regardless of the incident angle; in addition, the corresponding FFs were both maintained at 50%. Fig. 5c reveals that the measured value of J_{SC} under the TE-polarized light decreased from 3.5 to 1.5 mA/cm^2 upon increasing the incident angle from 0° to 80°; this decrease in efficiency arose from the large interfacial reflectance of the TE-polarized light. The reflectance of the TM-polarized light decreased at large incident angles because of the Brewster angle effect. The value of J_{SC} under the TM-polarized light did not, however, increase as a result of the decrease reflectance; instead, it decreased from 3.5 to 2.0 mA/cm^2. Fig. 5d displays the efficiencies of the cell under TE- and TM-polarized light at various incident angles. The efficiency under TE-polarized light decreased dramatically, from 0.93 to 0.38, in response to the decrease in J_{SC}, due to the large interfacial reflection (cf. Figs. 4b and 5c). The efficiency under TM-polarized light decreased from 0.93 to 0.50, mainly as a result of the anisotropic absorption of the P3HT:PCBM film. Because the direction of the electric field of the TM-polarized light changed upon changing the incident angle, the anisotropic crystallinity of

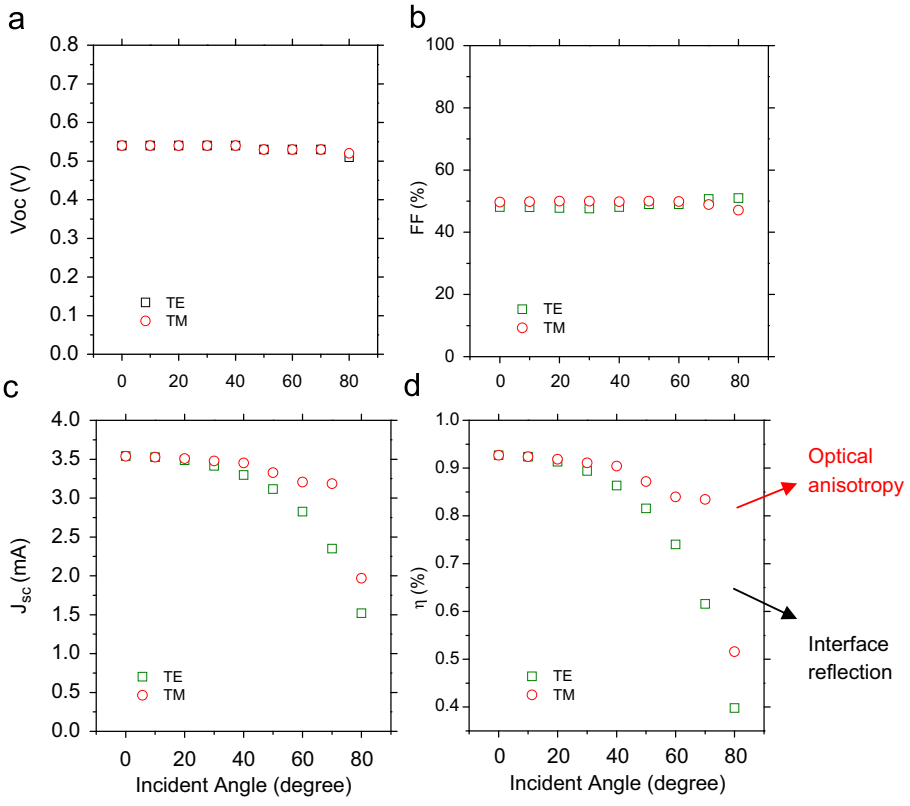

Fig. 5. Angle dependency of the values of (a) V_{OC}, (b) J_{SC}, (c) FF, and (d) η under TE- and TM-polarized light.

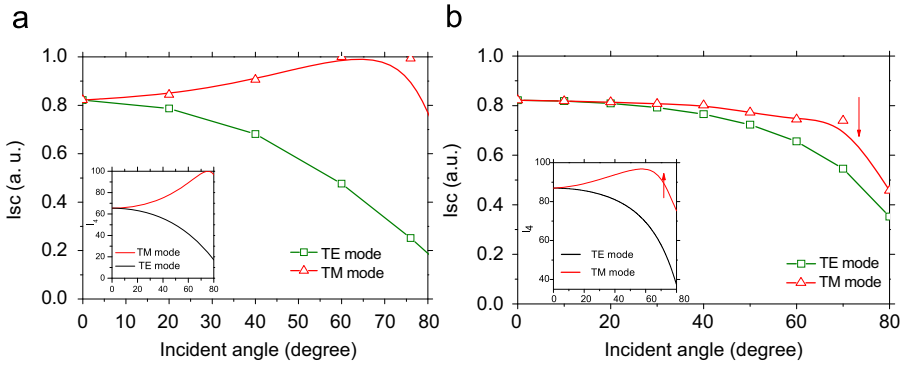

Fig. 6. Angle and polarization dependencies of the values of J_{SC} of (a) a Si solar cell and (b) an anisotropic P3HT:PCBM-based OPV. Insets: Interfacial transmittance under TE- and TM-polarized light.

P3HT:PCBM strongly reduced the absorption of TM-polarized light (Fig. 2d) at large incident angles and, therefore, decreased the values of J_{SC} and efficiency.

To verify that the anisotropic crystallinity of P3HT:PCBM caused the efficiency of the TM mode to decrease, we examined the behavior of a corresponding Si solar cell exhibiting only a slight degree of optical anisotropy [32]. Fig. 6a displays the normalized values of J_{SC} of this Si-based solar cell at various incident angles. The value of J_{SC} under TE-polarized light decreased from 0.8 to 0.2, with the interfacial transmittance (inset) decreasing from 65% to 17%, upon increasing the incident angle from 0° to 80°. In contrast, the value of J_{SC} under TM-polarized light increased upon increasing the incident angle because of the relatively high interfacial transmittance (or low surface reflectance) of TM-polarized light at large incident angles, due to the Brewster angle effect. Fig. 5b displays the normalized values of J_{SC} for the large optical anisotropy of the P3HT:PCBM-based organic solar cell at various incident angles; the inset displays its interfacial transmittance. Similar to the behavior of the Si solar cell, the value of J_{SC} of the organic solar cell under TE-polarized light decreased from 0.80 to 0.36 upon increasing the incident angle—again, as a result of interfacial reflection. In contrast to the behavior of the Si solar cell, the value of J_{SC} under TM-polarized light decreased from 0.80 to 0.43 despite an increase in transmittance from 84% to 95%. The result clearly implies that the decrease in the value of J_{SC} arose mainly from the small absorption of TM-polarized light at large incident angles, due to the anisotropic crystallinity of the P3HT:PCBM films.

Bending or operating an OPV at a large incident angle influences its performance as a result of decreasing the interfacial transmittance and decreasing the absorption of TM-polarized light, due to optical anisotropy of the P3HT:PCBM film. To enhance the device efficiency when bending or illuminating at large incident angles, it is necessary to minimize the optical anisotropy of the P3HT:PCBM films and the interface reflection at large incident angles. Unfortunately, the anisotropic absorption of P3HT:PCBM films is an intrinsic property because the P3HT:PCBM blend tends to crystallize in a direction parallel to the substrate (i.e., in contrast to the electric field of TM-polarized light at large incident angles). Upon increasing the incident angle, the electric field of TM-polarized light is aligned increasingly perpendicular to the substrate, thereby decreasing the amount of light absorbed. This phenomenon results in high-crystallinity P3HT:PCBM exhibiting high optical anisotropy and, therefore, significantly reduced absorption of TM-polarized light at large incident angles. Unlike Si-based solar cells, organic solar cells based on P3HT:PCBM blend films exhibit an additional feature – anisotropic absorption – that strongly influences the efficiency under illumination at large incident angles. In this regard, a solution to the problem of external quantum efficiency loss at large incident angles would benefit the further development of organic solar cells. To enhance the absorption of TM-polarized light at large angles, one approach would be to crystallize the chains of P3HT:PCBM in the blend in a direction perpendicular to the substrate.

Of its three possible crystalline orientations [28], the most preferred orientation for P3HT is that in which its main chains lie in the plane of the substrate with the side chains presented vertically. This edge-on orientation is thermodynamically stable. Therefore, crystallizing P3HT:PCBM in a direction perpendicular to the substrate – a thermodynamically unstable orientation – would require additional processing steps. Vertical crystalline orientation of P3HT:PCBM blend maybe a solution to solve the external quantum efficiency loss of TM-polarized light at large incident angle. Tolbert et al. demonstrated that conjugated polymers are highly aligned when confined in mesoporous Si [35]. This finding suggests that the crystalline orientation of P3HT:PCBM blends might be adjustable through external confinement. The most convenient methods would be to confine P3HT:PCBM in nano-structures, such as mesoporous Si and anodic alumina (AAO) [36]. When a P3HT:PCBM blend adopts a crystalline orientation perpendicular to the vertically substrate, the vertically aligned P3HT:PCBM blend would exhibit improved charge transport. The direction of charge transport in organic solar cells is generally perpendicular to the substrate. Because P3HT main chains lie in the plane of the substrate, however, the mismatch between the charge transport direction and the orientation of the P3HT main chains may result in relatively low hole mobility. The hole mobility of a vertically crystalline P3HT:PCBM blend could be improved dramatically [36]. In addition, because the orientation of the main chains in a vertically crystalline P3HT:PCBM blend is consistent with the direction of the electric field of TM-polarized light at large incident angles, optical absorption could be enhanced.

On the other hand, an antireflection structure would be an alternative strategy for minimizing the efficiency loss due to large interfacial reflection at large incident angles. Many antireflective layers have been reported for Si-based solar cells, including multilayer optical thin films and textured structures [37]. Textured structures eliminate several of the problems arising from multilayer coatings, e.g., the selection of appropriate materials, layer-to-layer adhesion, and thermal mismatch or diffusion of one material into another [38,39]. Furthermore, wide-angle and broad-bandwidth antireflection is difficult to achieve in multilayer structures. In contrast, optimally textured structures generally provide wide-angle and broad-bandwidth antireflections; such textured structures in Si-based solar cell are typically fabricated using KOH or HF etching techniques. These chemical etching techniques are incompatible, however, with the plastic substrates of organic solar cells. Therefore, in this study we used nanoimprint lithography – a convenient and compatible

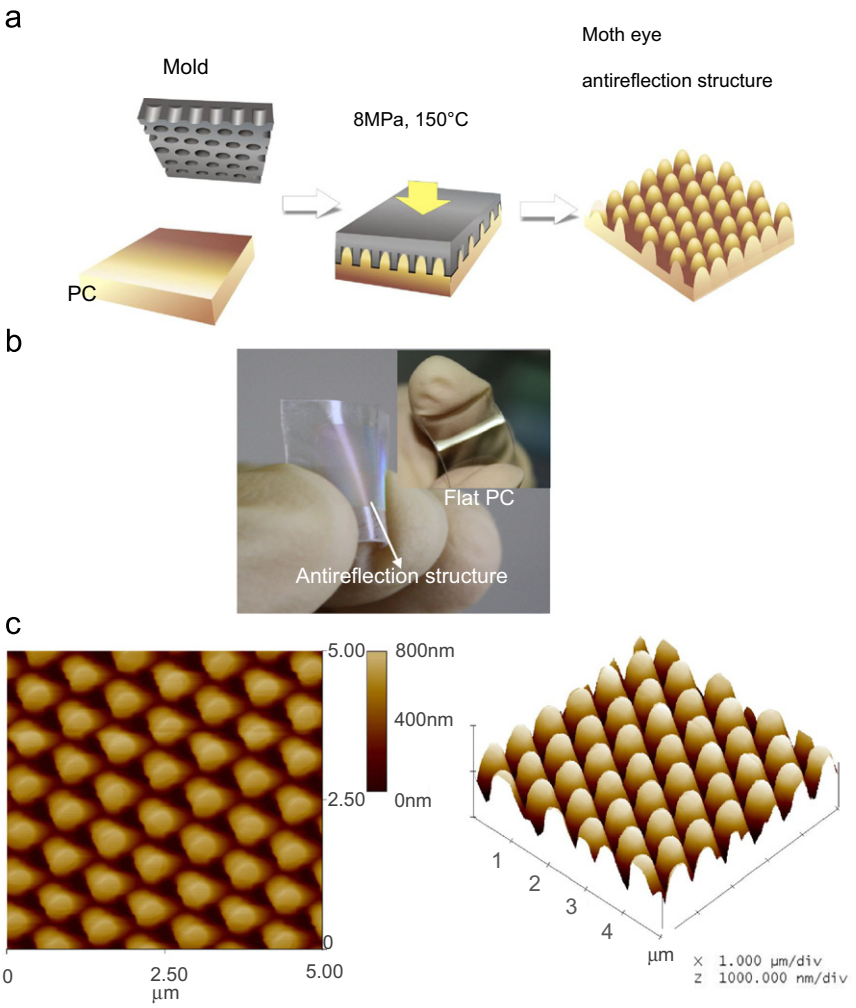

Fig. 7. (a) Schematic representation of the nanoimprint technique used to fabricate the antireflection structure. (b) Photographic image of the antireflection structure on a flexible PC substrate. (c) AFM image of the moth-eye structure having a base diameter of 400 nm, a height of 800 nm, and a period of 800 nm.

technique for flexible OPVs – to directly pattern antireflective moth-eye structures onto flexible PC substrates.

Fig. 7a provides a schematic representation of the fabrication of textured moth-eye structures on a flexible PC substrate. We used a Si mold having a period of 800 nm and a hole diameter of 400 nm to imprint the PC substrates at 150 °C and 8 MPa. This nanoimprint process provided moth-eye nanocone structures having the inverse pattern relative to the master mold structure. The photograph of the antireflection structure in Fig. 7b reveals the large difference in reflectance between the textured and flat regions on the PC substrates. The corresponding AFM image of the moth-eye structure (Fig. 7c) reveals a diameter of 400 nm, a height of 800 nm, and a period of 800 nm.

Fig. 8a displays the measured reflectance spectra of the PC substrates, in the presence and absence of the textured moth-eye structure, under TE- and TM-polarized light. For TE-polarized light, the textured structure exhibited a broadband antireflection relative to that of the flat PC substrate at an incident angle of 70°; the moth-eye textured structure featured a ca. 10% reflectance, significantly lower than that (40%) of the flat PC substrate, at this incident angle. For TM-polarized light, Fig. 8a reveals that the flat PC substrate exhibited low reflectance, due to the Brewster angle effect. After patterning the moth-eye structure onto the PC substrate, we observed a similar reflectance spectrum, implying that the moth-eye antireflection structure had only a slight effect on the TM-polarized light at large incident angles. Fig. 8b presents the angle-dependent reflectances of the structures under TE- and TM-polarized light. The textured PC substrate exhibited a wide-angle antireflection phenomenon for TE-polarized light; its reflectance decreased from 10% to 3% at normal incidence and from 45% to 10% at an incident angle of 70°. Under TM-polarized light, the reflectance of the PC substrates, both with and without the moth-eye structure, was ca. 5–10% at all incident angles. These results reveal that the moth-eye structure significantly reduced the reflectance of the TE-polarized light, causing more TE-polarized light to reach to the active layer when the textured structure was present on the PC substrate. Because of the optical anisotropy of P3HT:PCBM blend films at large incident angles, the absorption of TE-polarized light is much greater than that of TM-polarized light. By patterning the textured structure onto a PC substrate, the inefficient absorption of TE-polarized light, due to large angle reflection, can be alleviated. Our findings imply that moth-eye structures might enhance device efficiency when bent or operated at large incident angles because it would permit more TE-polarized light to enter the active layer. For a theoretical study, we employed the finite difference time domain (FDTD) method for near-field simulation. Fig. 8c displays the simulated results for a bent PC substrate prepared with and without the moth-eye antireflection structure. For an incident wavelength of 510 nm, the simulations reveal an obvious reflection of light above the

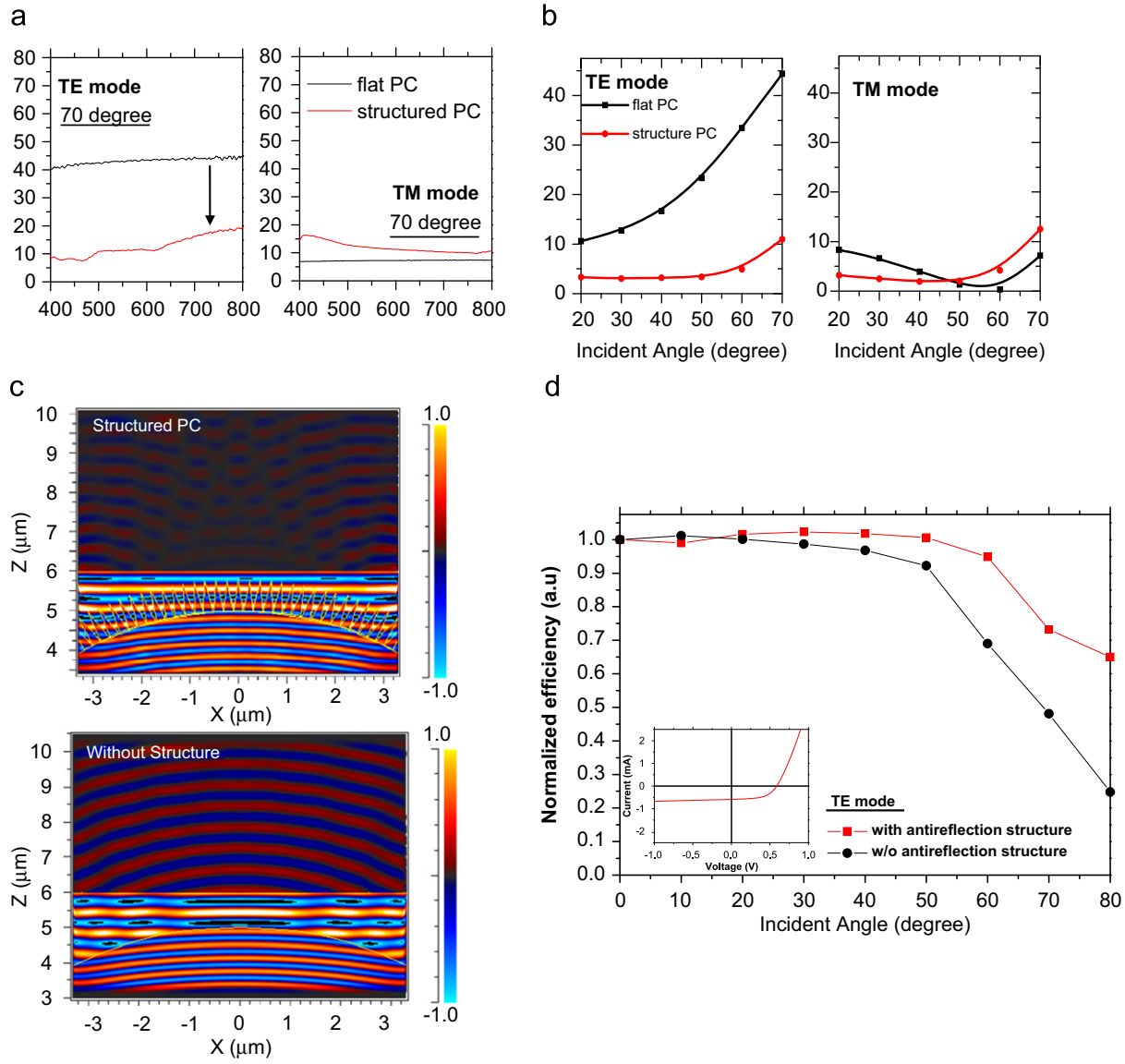

Fig. 8. (a) Wavelength dependencies of the TE- and TM-polarized reflectance spectra of PC substrates, prepared with and without a textured structure, at an incident angle of 70°. (b) Angle dependencies of the TE- and TM-polarized reflectances of PC substrates, prepared with and without a textured structure, at a wavelength of 510 nm. (c) FDTD simulation of the reflection of light from bent PC substrates prepared with and without a textured structure. (d) Angle dependency of the normalized efficiencies of the devices with and without an antireflection structure under TE-polarized light. Inserted graph is the *I–V* curve of the device with an antireflection structure under normal incidence (V_{OC}=0.59 V, I_{SC}=0.592 mA, FF=55.5, η=3.23).

bent substrate lacking the textured structure. For the textured, bent PC substrate, the amount of reflected light was minimal, consistent with our experimental measurements.

Finally, we further utilized the nanoimprint lithography to fabricate an antireflection structure for improving the efficiency of practical OPVs. The as-fabricated device has an efficiency of 3.23 under normal incidence. For the ease of comparison, we normalized the angle-dependent efficiency to that of normal incidence. Fig. 8d displays the normalized efficiency of the devices in the absence or presence of an antireflection structure under TE-polarized light illumination and the inserted graph was the *IV*-curve of the device under normal incidence. At incident angles smaller than 20°, both devices exhibit similar efficiencies due to the low reflectance of a PC substrate at small incidence angles. As increasing the incident angle, however, the functioning of the antireflection structure was apparently observed. The normalized efficiency of the device with an antireflection structure maintained 0.95 at 60°, and still remained a high value of 0.65 even at 80°. In contrast, the normalized efficiency of the device without an antireflection structure strongly decreased to 0.69 at 60°, and further dropped to 0.24 at 80°. The experimental results indicated that a moth-eye textured antireflection structure could effectively increase the efficiency of P3HT:PCBM-based OPVs at large incident angles.

4. Conclusions

The combination of optical anisotropy of P3HT:PCBM blend films and interfacial reflection results in a loss of external efficiency for organic solar cells that are bent or illuminated at large incident angles. The measured efficiencies of such devices decrease significantly at large incident angles—especially under TM-polarized light, where anisotropic absorption of the active layer occurs, in contrast to the increased efficiency of Si-based solar cells. Simulations of the reflectance at multiple interfaces revealed that light was reflected mostly at the outermost air–flexible substrate interface, due to its largest refractive index

difference. To alleviate this reflection loss, we used nanoimprint lithography to fabricate textured antireflection structures on flexible substrates. Experimental results and simulations confirmed that the presence of the textured structures led to obvious reductions in the degrees of interfacial reflection under TE-polarized light. As a result, more TE-polarized light, which is absorbed strongly in P3HT:PCBM films, can reach to the active layer of the OPV. An obvious efficiency enhancement was observed at oblique incidence when the device was made with a moth-eye antireflection structure. Therefore, we would expect the increased efficiency of such textured organic solar cells when they are bent or illuminated at large incident angles.

Acknowledgment

We thank the National Science Council, Taiwan, ROC, for supporting this study under contracts NSC-97-2221-E-002-046-MY3 and 98-2623-E-002 -001-ET.

References

[1] K.M. Coakley, M.D. McGehee, Conjugated polymer photovoltaic cells, Chem. Mater. 16 (2004) 4533–4542.
[2] B.P. Rand, J. Genoe, P. Heremans, J. Poortmans, Solar cells utilizing small molecular weight organic semiconductors, Prog. Photovolt.: Res. Appl. 15 (2007) 659–676.
[3] J.Y. Kim, K. Lee, N.E. Coates, D. Moses, T.Q. Nguyen, M. Dante, A.J. Heegar, Efficient tandem polymer solar cells fabricated by all-solution processing, Science 317 (2007) 222–225.
[4] J.U. Lee, A. Cirpan, T. Emrick, T.P. Russell, W.H. Jo, Synthesis and photophysical property of well-defined donor–acceptor diblock copolymer based on regioregular poly(3-hexylthiophene) and fullerene, J. Mater. Chem. 19 (2009) 1483–1489.
[5] G. Yu, J. Gao, J.C. Hummelen, F. Wudl, A.J. Heeger, Polymer photovoltaic cells: enhanced efficiencies via a network of internal donor-acceptor heterojunctions, Science 270 (1995) 1789–1791.
[6] G. Dennler, M.C. Scharber, C.J. Brabec, Polymer–fullerene bulk-heterojunction solar cells, Adv. Mater. 21 (2009) 1323–1338.
[7] L.M. Chen, Z. Hong, G. Li, Y. Yang, Recent progress in polymer solar cells: manipulation of polymer: fullerene morphology and the formation of efficient inverted polymer solar cells, Adv. Mater. 21 (2009) 1434–1449.
[8] M. Campoy-Quiles, T. Ferenczi, T. Agostinelli, P.G. Etchegoin, Y. Kim, T.D. Anthopoulos, P.N. Stavrinou, D.D.C. Bradley, J. Nelson, Morphology evolution via self-organization and lateral and vertical diffusion in polymer: fullerene solar cell blends, Nat. Mater. 7 (2008) 158–164.
[9] W. Ma, C. Yang, X. Gong, K. Lee, A.J. Heeger, Thermally stable, efficient polymer solar cells with nanoscale control of the interpenetrating network morphology, Adv. Funct. Mater. 15 (2005) 1617–1622.
[10] G. Li, V. Shrotriya, J. Huang, Y. Yao, T. Moriarty, K. Emery, Y. Yang, High-efficiency solution processable polymer photovoltaic cells by self-organization of polymer blends, Nat. Mater. 4 (2005) 864–868.
[11] J. Huang, G. Li, Y. Yang, A semi-transparent plastic solar cell fabricated by a lamination process, Adv. Mater. 20 (2008) 415–419.
[12] F.C. Krebs, S.A. Gevorgyan, J. Alstrup, A roll-to-roll process to flexible polymer solar cells: model studies, manufacture and operational stability studies, J. Mater. Chem. 19 (2009) 5442–5451.
[13] M. Al-Ibrahim, H.K. Roth, S. Sensfuss, Efficient large-area polymer solar cells on flexible substrates, Appl. Phys. Lett. 85 (2004) 1481–1483.
[14] H. Kim, W.W. So, S.J. Moon, The importance of post-annealing process in the device performance of poly(3-hexylthiophene): Methanofullerene polymer solar cell, Sol. Energy Mater. Sol. Cells 91 (2007) 581–587.
[15] G. Li, Y. Yao, H. Yang, V. Shrotriya, G. Yang, Y. Yang, "Solvent annealing" effect in polymer solar cells based on poly(3-hexylthiophene) and methanofullerenes, Adv. Funct. Mater. 17 (2007) 1636–1644.
[16] V.D. Mihailetchi, H. Xie, B. de Boer, L.J.A. Koster, P.W.M. Blom, Charge transport and photocurrent generation in poly(3-hexylthiophene): methanofullerene bulk-heterojunction solar cells, Adv. Funct. Mater. 16 (2006) 699–708.
[17] A. Saeki, S. Seki, Y. Koizumi, T. Sunagawa, K. Ushida, S. Tagawa, Increase in the mobility of photogenerated positive charge carriers in polythiophene, J. Phys. Chem. B 109 (2005) 10015–10019.
[18] Z. Xu, L.M. Chen, G. Yang, C.H. Huang, J. Hou, Y. Wu, G. Li, C.S. Hsu, Y. Yang, Vertical phase separation in poly(3-hexylthiophene): fullerene derivative blends and its advantage for inverted structure solar cells, Adv. Funct. Mater. 19 (2009) 1227–1234.
[19] B.Y. Yu, A. Tsai, S.P. Tsai, K.T. Wong, Y. Yang, C.W. Chu, J.J. Shyue, Efficient inverted solar cells using TiO_2 nanotube arrays, Nanotechnology 19 (2008) 255202-1–255202-5.
[20] J. JO, S.I. Na, S.S. Kim, T.W. Lee, Y. Chung, S.J. Kang, D. Vak, D.Y. Kim, Three-dimensional bulk heterojunction morphology for achieving high internal quantum efficiency in polymer solar cells, Adv. Funct. Mater. 19 (2009) 2398–2406.
[21] H. Mousazadeh, A. Keyhani, A. Javadi, H. Mobli, K. Abrinia, A. Sharifi, A review of principle and sun-tracking methods for maximizing solar systems output, Renewable Sustainable Energy Rev. 13 (2009) 1800–1818.
[22] D. Comoretto, R. Tubino, G. Dellepiane, G.F. Musso, A. Borghesi, A. Piaggi, G. Lanzani, Optical properties of highly oriented fibrous polyacetylene, Phys. Rev. B 41 (1990) 3534–3539.
[23] M. Tammer, A.P. Monkman, Measurement of the anisotropic refractive indices of spin cast thin poly(2-methoxy-5-(2′-ethyl-hexyloxy)-p-phenylenevinylene) (MEH–PPV) films, Adv. Mater. 14 (2002) 210–212.
[24] C.M. Ramsdale, N.C. Greenham, Ellipsometric determination of anisotropic optical constants in electroluminescent conjugated polymers, Adv. Mater. 14 (2002) 212–215.
[25] J.M. Winfield, C.L. Donley, J.S. Kim, Anisotropic optical constants of electroluminescent conjugated polymer thin films determined by variable-angle spectroscopic ellipsometry, J. Appl. Phys. 102 (2007) 063505-1–063505-7.
[26] U. Zhokhavets, G. Gobsch, H. Hoppe, N.S. Sariciftci, Anisotropic optical properties of thin poly(3-octylthiophene)-films as a function of preparation conditions, Synth. Met. 143 (2004) 113–117.
[27] C. Soci, D. Comoretto, F. Marabelli, D. Moses, Anisotropic photoluminescence properties of oriented poly(p-phenylene-vinylene) films: effects of dispersion of optical constants, Phys. Rev. B 75 (2007) 075204-1–075204-11.
[28] Y. Kim, S. Cook, S.M. Tuladhar, S.A. Choulis, J. Nelson, J.R. Durrant, D.D.C. Bradley, M. Giles, I. Mcculloch, C.S. Ha, M. Ree, A strong regioregularity effect in self-organizing conjugated polymer films and high-efficiency polythiophene:fullerene solar cells, Nat. Mater. 5 (2006) 197–203.
[29] M. Aryal, K. Trivedi, W. Hu, Nano-confinement induced chain alignment in ordered P3HT nanostructures defined by nanoimprint lithography, ACS-Nano 3 (2009) 3085–3090.
[30] B. Meredig, A. Salleo, R. Gee, Ordering of poly(3-hexylthiophene) nanocrystallites on the basis of substrate surface energy, ACS-Nano 3 (2009) 2881–2886.
[31] S.Y. Chuang, H.L. Chen, W.H. Lee, Y.C. Huang, W.F. Su, W.M. Jen, C.W. Chen, Regioregularity effects in the chain orientation and optical anisotropy of composite polymer/fullerene films for high-efficiency, large-area organic solar cells, J. Mater. Chem. 19 (2009) 5554–5560.
[32] T. Erb, U. Zhokhavets, G. Gobsch, S. Raleva, B. Stuhn, P. Scilinsky, C. Waldauf, C.J. Barbec, Correlation between structural and optical properties of composite polymer/fullerene films for organic solar cells, Adv. Funct. Mater. 15 (2005) 1193–1196.
[33] H.A. Macleod, Thin Film Optical Filters, Institute of Physics Publishing, 2001, pp. 418-436.
[34] A.J. Moule, J.B. Bonekamp, K. Meerholz, The effect of active layer thickness and composition on the performance of bulk-heterojunction solar cells, J. Appl. Phys. 100 (2006) 094503-1–094593-7.
[35] T.Q. Nguyen, J. Wu, S.H. Tolbert, B.J. Schwartz, Control of energy transport in conjugated polymers using an ordered mesoporous silica matrix, Adv. Mater. 13 (2001) 609–611.
[36] K.M. Coakley, B.S. Srinivasan, J.M. Ziebarth, C. Goh, Y. Liu, M.D. McGehee, Enhanced hole mobility in regioregular polythiophene infiltrated in straight nanopores, Adv. Funct. Mater. 15 (2005) 1927–1932.
[37] H.L. Chen, S.Y. Chuang, C.H. Lin, Y.H. Lin, Using colloidal lithography to fabricate and optimize sub-wavelength pyramidal and honeycomb structures in solar cells, Opt. Express 15 (2007) 14793–14803.
[38] P. Lalanne, G.M. Morris, Antireflection behavior of silicon subwavelength periodic structures for visible light, Nanotechnology 8 (1997) 53–56.
[39] C.H. Sun, B. Ho, J.B. Jiang, P. Jiang, Biomimetic subwavelength antireflective gratings on GaAs, Opt. Lett. 33 (2008) 2224–2226.